I.O. Goroshko[1], Y.A. Zhuk[1], A.S. Fallah[2], P. Sareh[3]

DYNAMIC BEHAVIOUR OF COMPOSITE WIND TURBINE BLADES WITH DIFFERENT MATERIAL COMBINATIONS: A NUMERICAL STUDY

[1]Department of Theoretical and Applied Mechanics, Taras Shevchenko National University of Kyiv, Kyiv 01601, Ukraine; e-mail: igoroshko@ukr.net; y.zhuk@i.ua

[2]Oslo Metropolitan University, P.O. Box 4, St. Olavs plass, NO-0130 Oslo, Norway; e-mail: arashsol@oslomet.no

[3] Creative Design Engineering Lab (Cdel), School of Engineering, University of Liverpool, Liverpool L69 3GH, United Kingdom; e-mail: pooya.sareh@liverpool.ac.uk

Abstract. This article reports the numerical simulation and analysis of the dynamic behaviour of the rotor blades of horizontal axis wind turbines made of different composite materials with different stacking layups. This type of wind turbine is dominant in modern high-power wind energy plants, and its dynamic characteristics should be carefully studied. For the purpose in this paper, computer models of rotor blades with composite skins with different structures and stiffeners were developed and studied using the finite element method (FEM). On the basis of these models, the modal analysis of turbine blade vibrations was performed, and the benchmark cases for the dynamic response under a uniform sine-pulse pressure applied to the underneath part of the blade were investigated by finite element calculations.

Keywords: horizontal axis wind turbines, rotor blades, layered composites, finite element simulation, modal analysis, pulse loading, dynamic response.

Introduction.

Today, wind energy, along with solar energy, is considered a predominant source of ‘green’ electricity. Wind power is currently the fastest growing renewable energy sector and makes a substantial contribution to reducing greenhouse gases and achieving the emissions reduction targets set by the Kyoto Protocol and Paris Agreements. Furthermore, the rapidly developing improvements in wind turbine performance and efficiency increase their economic competitiveness compared to conventional power-generating technologies [8].

In recent decades, in the evolution of wind energy technology, the main tendency has been to grow the size of wind turbine rotors. This is driven by both economic and technological demands as larger turbines have enhanced performance and increased production capacity required for new wind power plants [7, 10]. In turn, scaling up wind turbines leads to new complex problems in the design and operation of single turbines as well as wind farm spacing. The solution of these problems along with experimental investigations requires intensive computer simulations of the dynamic processes in all the wind turbine parts, especially in the blades, which in the case of large turbines are now made of composite materials and have a rather complex structure. Modern turbines have substantially longer blades than their predecessors (tens of metres) and are much more flexible. These blades are designed as long slender composite shell structures with stiffeners that are substantially inhomogeneous and slenderising towards the tip. This necessitates a variety of studies on the structural dynamics of such blades to evaluate deformations and stresses in their structures. Possible intensive vibrations in service conditions can not only

cause fatigue damage and affect structural strength and stability, but also have a substantial influence on power production [3]. Additionally, the simulation of dynamic processes is necessary in the vibration control of wind turbines [8, 9].

For the computer simulation of their dynamic behaviour, a number of modern FEM packages are widely used. They allow us to build models of blades with high accuracy and simulate their dynamic behaviour, taking into account nonlinear geometric and material effects.

In this paper, the mechanical models of horizontal axis wind turbine (HAWT) rotor blades of different composite skin structures with stiffeners were developed and implemented using the finite element package ABAQUS [1]. On this basis, modal analysis was carried out on blade vibrations, and benchmark cases for the dynamic response were investigated. The response of the system subjected to uniform pressure underneath of a half-sine shape was studied in detail. The blade tip displacement time histories were obtained from the results of finite element simulations.

§1. Finite element models of the blades.

To investigate the response of real rotor blades made of composite materials with different stacking layups, the corresponding finite element models were developed to be consistent with industry demands. They consist of composite skin and wooden stiffeners and incorporate all necessary FEM modelling environments for effective modal analysis and simulation of transient blade response to different types of loading. The blade geometry is obtained from a modified version [4] of a 3-MW turbine proposed in [5], which uses a scale-up version of a 20.15 m long blade in [2]. The geometry of the blade is shown in Fig. 1. The rotor blade, which is 44.175 m long, has a circular cross-section from its root attaching the rotor hub to the 1.753-metre span location. Then, the circular blade cross-sections gradually transition to airfoil sections that have NREL airfoil types S818 at the 9.648-metre, S825 at the 32.667-metre, and S826 at the 41.873-metre and 44.175-metre span locations. Table 1 presents the details of the cross-sections framing the blade [4], the basis of the finite element model of which was developed earlier in [6].

The material constitutive parameters for glass fibre-reinforced polymers (GFRPs) are given in Table 2, and those for carbon fibre-reinforced polymers (CFRPs) are given in Table 3. The blade was enforced with a wooden stiffener (longleaf pine [11]) with the density, stiffness moduli and Poisson's ratios listed in Table 4. The stiffener is chosen to run along the entire blade, as shown in the rear view of the blade root in Fig. 2.

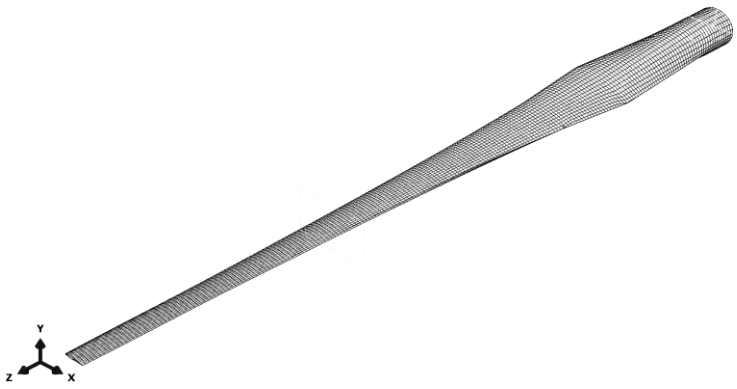

Fig. 1

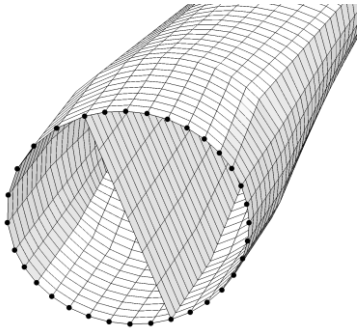

Fig. 2

Table 1. Section thicknesses along the beam axis
(measured from the circular root)

Section number	Distance from the root in the z-direction (mm)	Thickness t (mm)
1	1,754	96.02
2	9,648	79.04
3	14,251	53.21
4	29,212	13.44
5	44,175	10.34

Table 2. Stiffness moduli and Poisson's ratios for the GFRP composite
(1 – fibre direction; 2 – transverse direction; 3 – through-the-thickness direction)

ρ (kg/m^3)	E_1 (GPa)	E_2 (GPa)	E_3 (GPa)	ν_{12}	ν_{13}	ν_{23}	G_{12} (GPa)	G_{13} (GPa)	G_{23} (GPa)
1860	37.0	18.0	18.0	0.25	0.25	0.3	8.0	8.0	6.9

Table 3. Stiffness moduli and Poisson's ratio
for the CFRP composite (lamina format)

ρ (kg/m^3)	E_1 (GPa)	E_2 (GPa)	ν_{12}	G_{12} (GPa)	G_{13} (GPa)	G_{23} (GPa)
1600	170.0	9.0	0.34	4.8	4.8	4.5

Table 4. Stiffness moduli and Poisson's ratios for the longleaf pine

ρ (kg/m^3)	E_1 (GPa)	E_2 (GPa)	E_3 (GPa)	ν_{12}	ν_{13}	ν_{23}	G_{12} (GPa)	G_{13} (GPa)	G_{23} (GPa)
590	15.07	1.537	0.829	0.332	0.365	0.384	1.07	0.904	0.181

§2. Modal analysis of the blade vibrations.

Here, we consider how the properties of composite materials and the way their layers are stacked affect the spectrum of the eigenmodes of the wind turbine blade. The results of computations of the natural frequencies (in Hz) for blades with skin made of glass fibre-reinforced composites (GFRCs) with different layup orientations and wooden stiffeners with a thickness of 75 mm are presented in Table 5. The type of movement is indicated in the table near the frequency values in parentheses: F is for flap vibrations, L is for lead-lag vibrations, and T is for torsional vibrations; in the cases of combined movements, more than one indicator is used. The shapes of the eigenmodes obtained for the case of the unidirectional composite (UD) are shown in Fig. 3. The eigenfrequencies together with the shapes of the modes for the blades with 0/90/0/90/0 and 0/−30/30/90/0 layups are close, which leads to a similarity in their dynamic behaviour, as we will see in the next section.

Table 5. Natural frequencies (in Hz) for blades with skin made of GFRCs with different layup orientations and wooden stiffeners with a thickness of 75 mm

N_{mode}	UD	0/90/0/90/0	0/−45/45/90/0	0/−30/30/90/0
1	0.5135 (F)	0.4633 (F)	0.4470 (F)	0.4642 (F)
2	1.7487 (F)	1.5791 (FL)	1.5243 (FL)	1.5824 (FL)
3	2.2151 (LF)	1.9831 (FL)	1.9086 (FL)	1.9898 (FL)
4	4.0711 (F)	3.6877 (F)	3.5658 (F)	3.6970 (F)
5	6.6857 (FL)	6.0515 (FL)	5.8523 (FL)	6.0749 (FL)
6	7.2677 (FL)	6.5787 (FL)	6.3662 (FL)	6.6059 (FL)
7	9.7345 (FT)	8.9108 (F)	8.6587 (F)	8.9485 (F)
8	9.8190 (T)	9.8253 (T)	10.6351 (T)	10.4369 (T)
9	12.6217 (LF)	11.4563 (FL)	11.1188 (FLT)	11.5332 (FL)

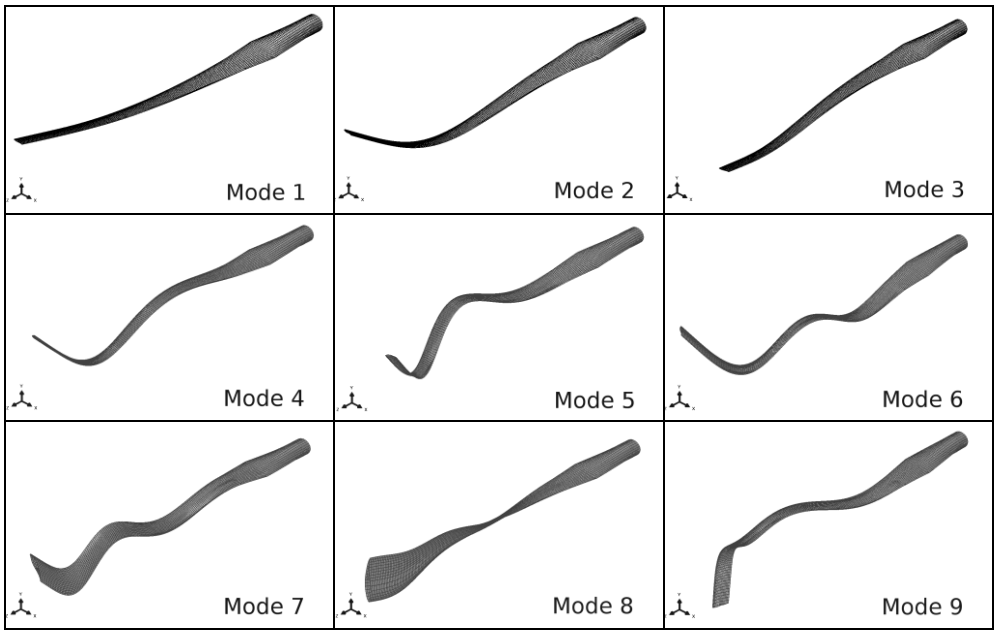

Fig. 3

In Table 6, the eigenfrequencies and types of movement for blades with skin made of the carbon fibre-reinforced composite (CFRC) with different layup orientations and the same wooden stiffener are given. Here, we observe a closeness within the eigenfrequencies and shapes of the modes for the 0/90/0/90/0 and 0/−30/30/90/0 layups up to the 4th mode.

Table 6. Eigenfrequencies and types of motion for blades with skin made of CFRC with different layup orientations and wooden stiffeners with a thickness of 75 mm

N_{mode}	UD	0/90/0/90/0	0/−45/45/90/0	0/−30/30/90/0
1	1.1220 (F)	0.8989 (F)	0.8120 (F)	0.9013 (F)
2	3.6862 (F)	3.0077 (FL)	2.7615 (FL)	3.0514 (FL)
3	4.8182 (FL)	3.9008 (FL)	3.5766 (FL)	3.9774 (FL)
4	7.9795 (FT)	6.7688 (F)	6.4064 (F)	7.0162 (F)
5	8.3539 (T)	8.3824 (T)	10.5700 (FL)	11.4411 (FL)
6	12.1746 (FL)	10.8617 (FL)	11.6113 (FL)	12.6832 (FL)
7	13.4381 (LT)	11.8192 (FL)	15.1609 (F)	14.6171 (T)
8	14.5928 (T)	15.0714 (FT)	16.1947 (T)	16.1197 (FL)
9	16.0189 (FT)	15.0947 (T)	20.2028 (FL)	21.2836 (FL)

Table 7 presents the eigenfrequencies and types of movement for blades in which the following combination of materials is used: the first three sections with the thickest walls

are made of GFRC, and the thin-walled fourth and fifth sections are made of CFRC. The layup orientations and wooden stiffener are the same as in previously considered cases. For this type of material distribution in the blade, a closeness within the eigenfrequencies and shapes of the modes for the 0/90/0/90/0 and 0/−30/30/90/0 layups up to the 4th mode, as in the previous pure CFRC case, also takes place.

Table 7. Eigenfrequencies and types of motion for blades made of a combination of materials

N_{mode}	UD	0/90/0/90/0	0/−45/45/90/0	0/−30/30/90/0
1	1.0401 (F)	0.8491 (F)	0.7738 (F)	0.8509 (F)
2	3.1492 (FL)	2.6483 (FL)	2.4699 (FL)	2.6794 (FL)
3	3.8835 (FL)	3.2875 (FL)	3.0773 (FL)	3.3313 (FL)
4	6.8234 (FL)	5.8466 (FL)	5.5463 (F)	5.9742 (FL)
5	8.3326 (T)	8.3846 (T)	8.2098 (FL)	8.8029 (FL)
6	10.0380 (FL)	8.6464 (FL)	8.9066 (FL)	9.5123 (FL)
7	10.6198 (FL)	9.2965 (FL)	12.8006 (F)	13.6360 (FT)
8	14.1889 (FT)	13.0136 (FL)	15.9689 (T)	14.4969 (T)
9	14.6756 (T)	15.0877 (T)	16.5823 (FLT)	17.8008 (FLT)

§3. Investigation of the dynamic behaviour of the blade under pulse loading.

3.1. Half-sine pulse loading.

Consider now the results of the finite element simulation of the dynamic behaviour of wind rotor blades made of different composite materials and different layups in the case of loading from a uniform underneath pressure pulse of the half-sine shape with a 4-second duration which imitates the load at a wind gust.

To estimate the influence of geometrical nonlinearity on the simulation results in the case of skin made of unidirectional glass fibre-reinforced composites, corresponding computations were run for different load magnitudes. The first one was performed while applying the ABAQUS model accounting for geometrical nonlinearity, while the linear elastic ABAQUS model was employed for the second simulation.

The results for the blade tip point deflection time history in the *y* (flap) direction are shown in Fig. 4, where solid lines correspond to linear simulations and dashed lines correspond to those when nonlinear geometrical effects were included. The number labels in the figure represent the levels of the pressure load magnitude: (1) 10^2 Pa, (2) 5×10^2 Pa, (3) 7.5×10^2 Pa, and (4)10^3 Pa. These results show that for rather high load magnitudes up to 7.5×10^2 Pa, the influence of nonlinearity is negligible, and in further computations, we will use only linear models.

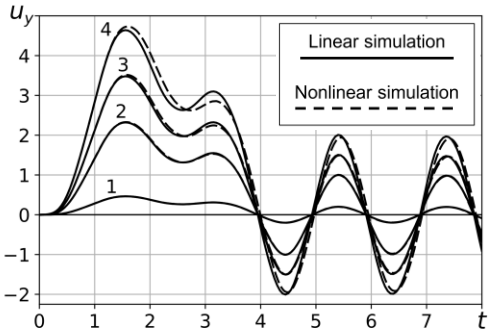

Fig. 4

Fig. 5 shows the displacements of the blade tip in the flap direction at a pressure magnitude of 100 Pa for the case of glass fibre-reinforced composite (GFRC) skins. The solid line corresponds to the unidirectional (UD) composite, the dashed line corresponds to the 0/ −30/30/90/0, the dash-dotted line corresponds to 0/−45/45/90/0, and the dotted line

corresponds to 0/90/0/90/0 layup orientations. In Fig. 6, corresponding graphs for the case of carbon fibre-reinforced composite (CFRC) blade skins are presented, and in Fig. 7, graphs for the case of blades with a combined structure (GFRC/CFRC) are shown.

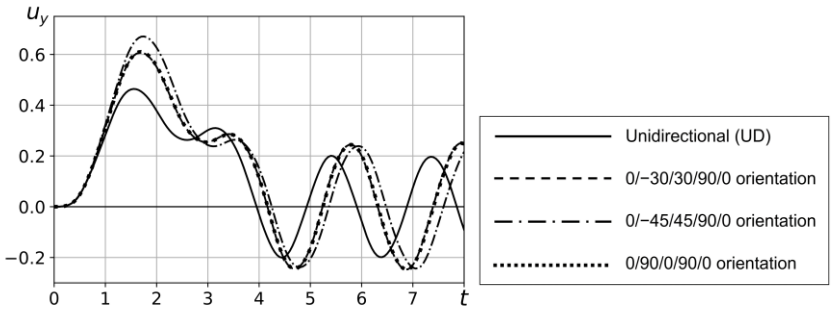

Fig. 5

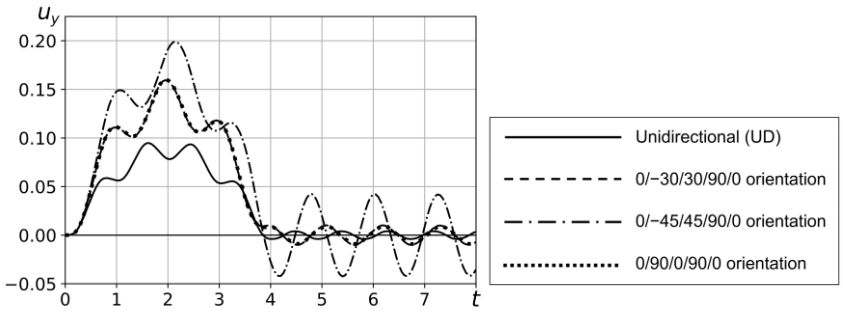

Fig. 6

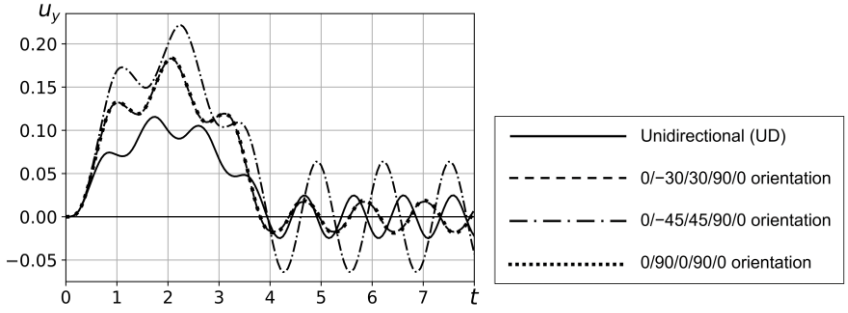

Fig. 7

In all the cases considered, we observe after the transition from the movement caused by the half-sine pulse of pressure to almost harmonic vibrations that correspond to the first bending flap modes, higher modes are practically not excited.

Because of the higher bending stiffness of the blades made of UD composites, we see essentially lower magnitudes of maximal displacements than in the other cases. Additionally, we observe a practical coincidence of vibrational movements for the cases of 0/−30/30/90/0 and 0/90/0/90/0 layups of composite skins, which should be expected due to the proximity of their lower eigenmodes, as noted in the previous section.

Since the nodal points of the mesh are not evenly distributed at the root of the blade (see Fig. 2), a special procedure was developed to find the corrected distribution of the reaction force results over the root circular cross-section. The distribution of the nodal values of the

reaction forces in Newtons is shown in Fig. 8, which corresponds to computations where geometrical nonlinearity was taken into account for a pressure loading magnitude of 10^3 Pa; this graph corresponds to the time t = 1.7s when the maximum values of the reaction forces were reached.

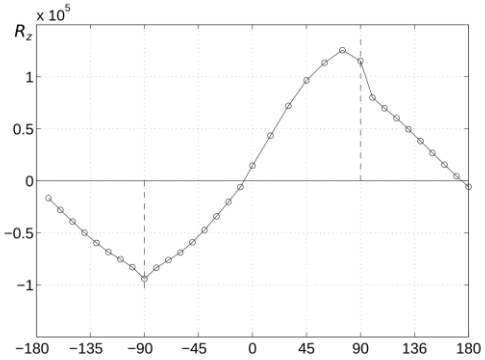

Fig. 8

To this end, the standard Fourier approximation was used:

$$
\begin{aligned}
f(x) &\approx \frac{a_0}{2} + \sum_{n=1}^{N} \left(a_n \cos nx + b_n \sin nx\right), \\
a_0 &= \frac{1}{\pi} \int_{-\pi}^{\pi} f(x)\, dx, \\
a_n &= \frac{1}{\pi} \int_{-\pi}^{\pi} f(x) \cos nx\, dx, \\
b_n &= \frac{1}{\pi} \int_{-\pi}^{\pi} f(x) \sin nx\, dx.
\end{aligned}
\tag{1}
$$

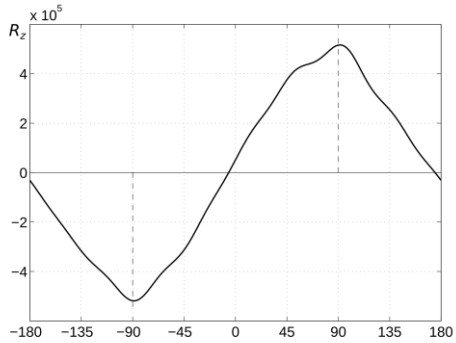

Fig. 9

The corrected results for the density of the membrane reaction force R_z (N/m) are shown in Fig. 9 for the UD composite skin and wooden stiffener composition, where the effect of the stiffener is clearly visible as the noticeable increase in the membrane reaction occurs at the places where the stiffener is attached (90° and −90°). This effect should be taken into account when the strength, fatigue resistance, and life prediction of the blade are evaluated.

3.2. Rectangular pulse loading.

In this subsection, we consider the results of computer simulations of the dynamic behaviour of wind rotor blades made of different composite materials and different layups in the case of loading by a uniform pressure pulse of a rectangular shape loaded underneath with a duration of 4 seconds.

Fig. 10 shows the displacements of the blade tip in the flap direction at a pressure magnitude of 100 Pa for the case of glass fibre-reinforced composite (GFRC) skins. The solid line corresponds to the unidirectional (UD) composite, the dashed line corresponds to the 0/−30/30/90/0 layup orientation, and the dash-dotted line corresponds to 0/−45/45/90/0 (hereinafter the results for the 0/90/0/90/0 layup are not presented because they are very close to the results for 0/−30/30/90/0 layup). In Fig. 11, corresponding graphs for the case of carbon fibre-reinforced composite (CFRC) blade skins are presented, and in Fig. 12, graphs for the case of blades with a combined structure (GFRC/CFRC) are shown.

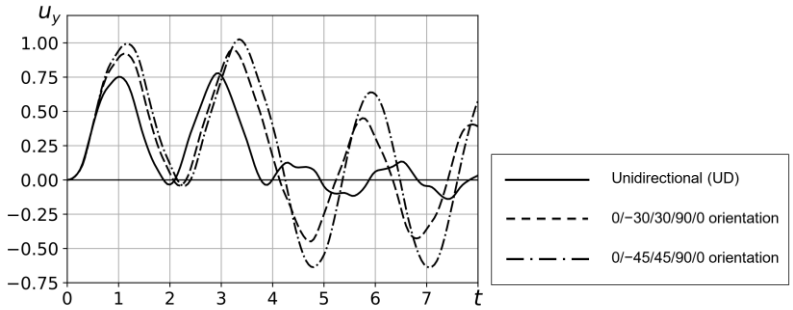

Fig. 10

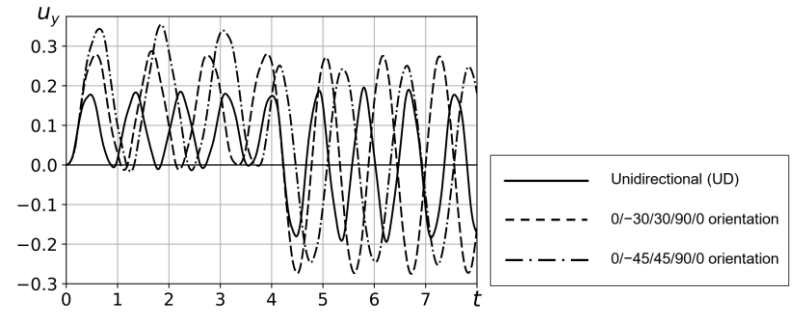

Fig. 11

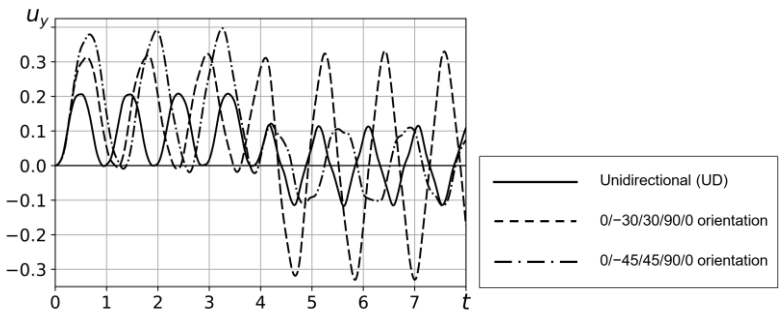

Fig. 12

3.3. Linearly-decaying triangular pulse loading.

In this subsection, the results of the computer simulation of the dynamic behaviour of wind rotor blades made of different composite materials and different layups in the case of loading underneath by a uniform linearly-decaying triangular pressure pulse with a duration of 4 seconds are considered.

Fig. 13 shows the displacements of the blade tip in the flap direction at a pressure magnitude of 100 Pa for the case of glass fibre-reinforced composite (GFRC) skins. The solid line corresponds to the unidirectional (UD) composite, the dashed line corresponds to the 0/−30/30/90/0 layup orientation, and the dash-dotted line corresponds to 0/−45/45/90/0. In Fig. 14, corresponding graphs for the case of carbon fibre-reinforced composite (CFRC) blade skins are presented, and in Fig. 15, graphs for the case of blades with a combined structure (GFRC/CFRC) are shown.

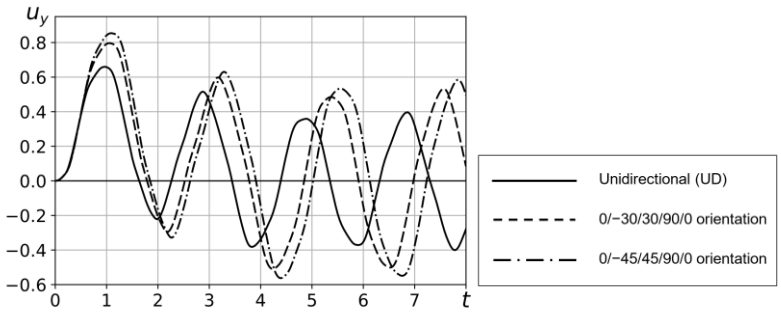

Fig. 13

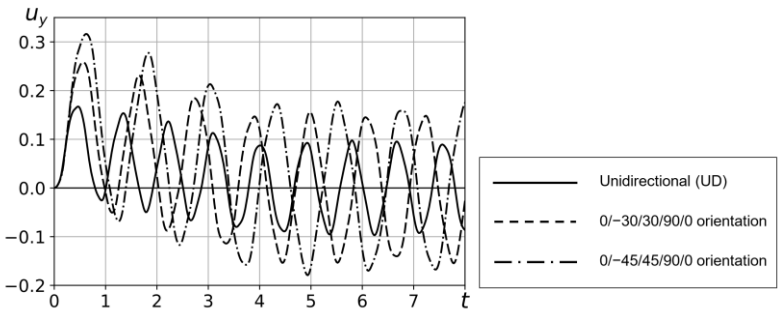

Fig. 14

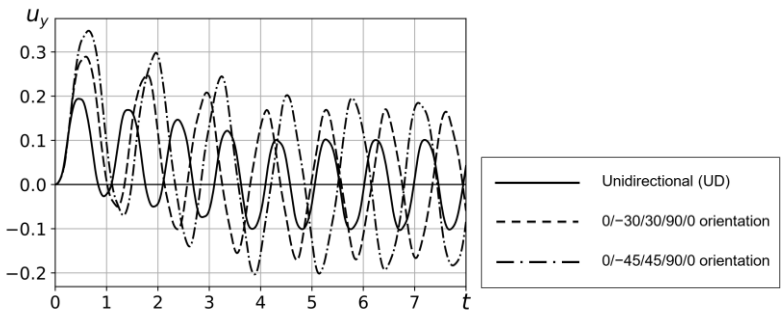

Fig. 15

Conclusions.

In this paper, mechanical models of horizontal axis wind turbine (HAWT) rotor blades made of glass and carbon fibre-reinforced composites with different stacking layups and wooden stiffeners using shell approximations were developed and implemented by means of the ABAQUS finite element package. The obtained models allow us to carry out a detailed investigation of the dynamic processes in the considered rotor blades.

The modal analysis of turbine blade vibrations demonstrated a wide variety of the shapes of the vibrational motion of the blade, from bending modes in the flap and lead-lag directions and their combinations to twisting modes.

In addition, the benchmark cases for the dynamic response were investigated for the half-sine shape pulse uniform pressure loading applied to the underneath part of the blade, which imitates the load of a wind gust, and for rectangular and linearly-decaying triangular pressure pulses. The computations were performed both in the linear and geometrically-nonlinear formulations. The blade tip displacement time histories were obtained from the results of finite element simulations. The results of the calculations showed that for up to some magnitude of the pressure (in the case of the unidirectional glass fibre-reinforced composite, the pressure is 7.5×10^2 Pa), the influence of nonlinearity is small and can be neglected.

Acknowledgements.

This work was partially supported by an ODA Research Seed Fund (2019/20) from the University of Liverpool.

1. ABAQUS. (2014). v. 6.14 User Guide.
2. *Bir G., Migliore P.* Preliminary structural design of composite blades for two- and three-blade rotors. – Technical Report NREL/TP-500-31486, National Renewable Energy Laboratory, Golden, Colorado, USA, 2004.
3. *Brondsted P., Nijssen R.P.L.* (eds.) Advances in Wind Turbine Blade Design and Materials. – Woodhead Publishing Limited, 2013. – 477 p.
4. *Chen K.-N., Chen P.-Y.* Structural optimization of 3 MW wind turbine blades using a two-step procedure // International Journal for Simulation and Multidisciplinary Design Optimization. – 2010. – N 4. – P. 159–165.
5. *Malcolm D.J., Hansen A.C.* WindPACT Turbine Rotor Design Study. – Subcontract Report NREL/SR-500-32495, National Renewable Energy Laboratory, Golden, Colorado, USA, 2006. – Retrieved from https://www.nrel.gov/docs/fy06osti/32495.pdf
6. *Navadeh, N., Goroshko, I.O., Zhuk, Y.A., Fallah, A.S.* An FEM-based AI approach to model parameter identification for low vibration modes of wind turbine composite rotor blades // European Journal of Computational Mechanics. – 2017. – **26**, N 5–6. – P. 541–556.
7. *Serrano-González J., Lacal-Arántegui R.* Technological evolution of onshore wind turbines – a market-based analysis. – Wind Energy. – 2016. – **19**. – P. 2171–2187. Retrieved from https://onlinelibrary.wiley.com/doi/full/10.1002/we.1974
8. *Staino A., Basu B.* Dynamics and control of vibrations in wind turbines with variable rotor speed. – 2013. – Engineering Structures. – **56**. – P. 58–67.
9. *Staino A., Basu B.* Emerging trends in vibration control of wind turbines: A focus on a dual control strategy // Philosophical Transactions of the Royal Society A. – 2015. **373**:20140069. – P. 1–16. – http://dx.doi.org/10.1098/rsta.2014.0069. – Retrieved from http://rsta.royalsocietypublishing.org/content/roypta/373/2035/20140069.full.pdf.
10. *Wiser R.H., Bolinger M.* 2015 Wind Technologies Market Report. – U.S. Department of Energy, 2016. – Retrieved from https://emp.lbl.gov/publications/2015-wind-technologies-market-report.

11. Wood Handbook – Wood as an engineering material. – General Technical Report FPL-GTR-190. Madison, WI: U.S. Department of Agriculture, Forest Service, Forest Products Laboratory – 2010. Retrieved from https://www.fpl.fs.fed.us/documnts/fplgtr/fpl_gtr190.pdf